



INVESTIGATION OF ELECTRONIC STRUCTURE OF CeO₂: FIRST PRINCIPLES CALCULATIONS

GAGAN AHUJA^a, SONU SHARMA^b and GUNJAN ARORA^{c*}

^aDepartment of Physics, Faculty of Science, PAHER University,
UDAIPUR – 313022 (Raj.) INDIA

^bDepartment of Physics, College of Science, M. L. Sukhadia University,
UDAIPUR – 313001 (Raj.) INDIA

^cDepartment of Physics, Geetanjali Institute of Technical Studies,
UDAIPUR – 313022 (Raj.) INDIA

ABSTRACT

In this paper, we present the first ever theoretical Compton profiles and electron momentum densities along with energy bands and density of states of rare earth oxide CeO₂. We have employed the linear combination of atomic orbitals method to compute these electronic properties. For this, we have applied local density approximation, generalized gradient approximation and recently developed second order generalized gradient approximation within the frame work of density functional theory. The energy band gap of CeO₂ is found to be in good agreement with the available data. Theoretical anisotropies in Compton profiles along [100], [110] and [111] directions are explained in terms of energy bands.

Key words: Band structure calculations, Density functional theory, Electron momentum density, Rare earth oxides.

INTRODUCTION

The rare-earth oxide CeO₂ (ceria) attracts much attention due to its technological and industrial applications. It is widely used in automobile exhaust as an oxygen storage material and catalyst due to its ability to take and release oxygen under oxidizing and reducing conditions. CeO₂ can be considered as a prospective material for future microelectronic applications due to its high dielectric constant and good epitaxy on Si. Further, CeO₂ is considered as a promising candidate for replacing silicon dioxide in electronic appliances¹. It crystallizes in fluorite like cubic structure as shown in Fig. 1.

* Author for correspondence; E-mail: garora.gits@gmail.com

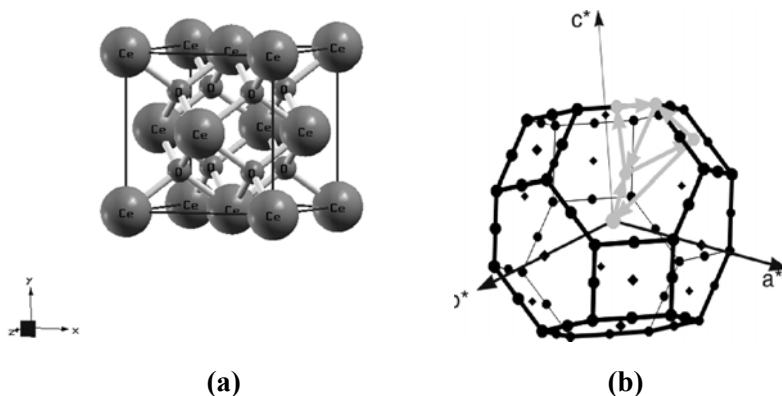


Fig. 1: (a) The crystalline structure of the cerium oxide (space group Fm3m, no. 225) along with (b) the reciprocal lattice

Earlier theoretical and experimental studies on CeO₂ mainly include quantum mechanical calculations, surface properties, elastic properties, X-ray diffraction measurements, electronic and optical properties¹⁻²⁹. Among recent studies, Babitha et al.¹⁷ have studied structural and optical properties of CeO₂ nanoparticles by chemical precipitation. Graciani et al.¹⁸ have reported the structural and electronic properties of CeO₂ and Ce₂O₃ using hybrid density functional theory (DFT). Keating et al.¹⁹ have determined the intrinsic defects properties within CeO₂. Low energy recoil events in MO₂ (M = Th, Ce and Zr) have been investigated by Xiao et al.²⁰ using *ab initio* molecular dynamics (MD) method. The structural, magnetic and optical properties of CeO₂, PrO₂ and TbO₂ have been undertaken by Kanoun et al.²¹ within the DFT framework based on full potential approaches. Desaunay et al.²² have reported the structural and electronic properties of CeO₂ using hybrid DFT method. High-pressure structural and electronic properties of CeO₂ and ThO₂ have been studied by Song et al.²³ with density functional calculations. The elastic constants, bulk modulus, shear modulus and elastic modulus of cubic fluorite CeO₂ under high pressure have been studied by Li et al.²⁴ using the plane-wave pseudo potential method based on DFT.

In the present paper, we have used first principles calculations to investigate electronic response of cerium oxide (CeO₂). The main objectives of the present work are (i) to compute the electronic band structure and density of states (DOS) of CeO₂ using more accurate second order generalized gradient approximation (GGA) and PBE sol parameters as embodied in linear combination of atomic orbitals (LCAO) (ii) to compute for the first time the electron momentum density (EMD) and Compton profiles (CPs) of CeO₂ using LCAO method (iii) to compute LCAO based anisotropies in theoretical CPs and analyze them in terms of energy bands and (v) to deduce more accurate band gap in CeO₂ and compare it with the available data.

Computational method

We have employed LCAO method, as incorporated in CRYSTAL09 code^{30,31} developed by Torino group, to compute the theoretical CPs, energy bands and DOS of CeO₂. It is worth mentioning that the CRYSTAL09 package includes various DFT schemes like local density approximation (LDA), GGA and second order GGA (so called SOGGA). In this code, the one electron crystalline orbitals are the linear combination of Bloch functions given as,

$$\Phi_i(\mathbf{r}, \mathbf{k}) = \sum \sum a_{\mu i}(\mathbf{k}) \Phi_{\mu}(\mathbf{r} - \mathbf{A}_{\mu} - \mathbf{g}) \exp(i\mathbf{k} \cdot \mathbf{g}) \quad \dots(1)$$

The Bloch functions, which are the solutions of one electron equations, are built from local atom by the linear combination of n_G individual Gaussian-type functions.

In the DFT scheme, the one particle Hamiltonian operator involves exchange and correlation potential operator $\hat{v}_{xc}(\mathbf{r})$, which is defined as –

$$\hat{v}_{xc}(\mathbf{r}) = \frac{\delta E_{xc}[n(\mathbf{r})]}{\delta \rho(\mathbf{r})} \quad \dots(2)$$

Here, E_{xc} is the exchange-correlation density functional energy and ρ is the electronic density at a point \mathbf{r} .

In LDA, the exchange-correlation energy of an electronic system is constructed by assuming that the exchange-correlation energy per electron at a point \mathbf{r} in the electron gas is equal to the exchange-correlation energy per electron in a homogenous electron gas that has the same electron density at the point \mathbf{r} . It follows that –

$$E_{xc}^{LDA}[n(\mathbf{r})] = \int n(\mathbf{r}) \varepsilon_{xc}[n(\mathbf{r})] d^3\mathbf{r} \quad \dots(3)$$

In the GGA, the appropriate exchange energy is formed from slowly varying densities is –

$$E_x^{GGA}[n(\mathbf{r})] = \int n(\mathbf{r}) \varepsilon_x^{LDA}(n(\mathbf{r})) F_x^{GGA}(s(\mathbf{r})) d^3\mathbf{r}, \quad \dots(4)$$

In Eq. 4, the variable s is the reduced density gradient, which is given by the formula,

$$s(n(\mathbf{r})) = \frac{|\nabla n(\mathbf{r})|}{2k_F n(\mathbf{r})}, \quad \dots(5)$$

and k_F is defined by $n(\mathbf{r}) = \frac{k_F^3}{3\pi^2}$.

The functional $F_X^{GGA}(s(\mathbf{r}))$ present in Eq. 4 is the exchange enhancement function of the GGA and in the case of PBE it is given by –

$$F_x^{PBE}(s) = 1 + \kappa - \frac{\kappa}{1 + \frac{\mu}{\kappa}s^2} \quad \dots(6)$$

where the constants are $\mu = 0.2195$ and $\kappa = 0.804$.

In the case of SOGGA, exchange enhancement factor is taken as equal mixing (50% each) of the PBE³² and revised PBE (RPBE)³³ exchange functionals. Mathematically,

$$F_x^{SOGGA} = 1 + \kappa \left(1 - \frac{1}{2} \frac{1}{1 + \frac{\mu s^2}{\kappa}} - \frac{1}{2} e^{-\mu s^2 / \kappa} \right) \quad \dots(6)$$

The parameters μ and K are redefined as $\mu = \mu^{GE} = 0.552$ and $K = 0.552$ using Lieb-Oxford bound³⁴.

In the present computations, we have taken exchange of Dirac-Slater^{30,31} for LDA and Wu and Cohen³⁵ and PBE sol³⁶ for GGA computations, whereas correlation function of PZ³³ for LDA and PBE³⁷ has been used for WCGGA, PBEsol and SOGGA. Due to the non-availability of all electron basis sets of Ce, we have used the pseudo potential (PP) basis sets from Kanoun et al.²¹, while all electrons Gaussian basis sets for O were taken from www.tcm.phy.cam.ac.uk/~mdt26/basis_sets. Here, in our study we have assumed that the f-orbitals are deeply occupied in the bulk, and can therefore be neglected in the Ce basis sets. The energy optimization of the basis sets was undertaken using the Billy software³¹. The tolerance on the total-energy convergence in the iterative solution of the Kohn–Sham equations is set to 10^{-6} Hartree. BRODYEN Scheme³⁸ was used to achieve fast convergence.

RESULTS AND DISCUSSION

Energy bands and density of states

We have computed the energy bands and DOS of CeO₂, using PP-DFT-LDA/PBEsol/WCGGA/SOGGA theories of LCAO method. In Figs. 2(a,b), we have

presented the energy bands and DOS using PP-DFT-SOGGA theory, as the overall shapes (except some fine structures and energy values) of energy bands computed using all the theories are almost same. Except some fine structures, our energy bands and DOS are seen to be in good agreement with the earlier reported data^{2,3,11,14,21,22}. As we have taken 4f-orbital in core part of Ce basis set so f orbital bands are absent in the shown energy range. The valence band maxima (VBM) and conduction band minima (CBM) exist at Γ point, which confirms the direct band gap character of CeO₂. In Fig. 2(b), the total and partial DOS for 6s, 5p and 5d valence electrons of Ce along with 2sp electrons of O are shown. Some salient features of energy bands and density of states are as follows:

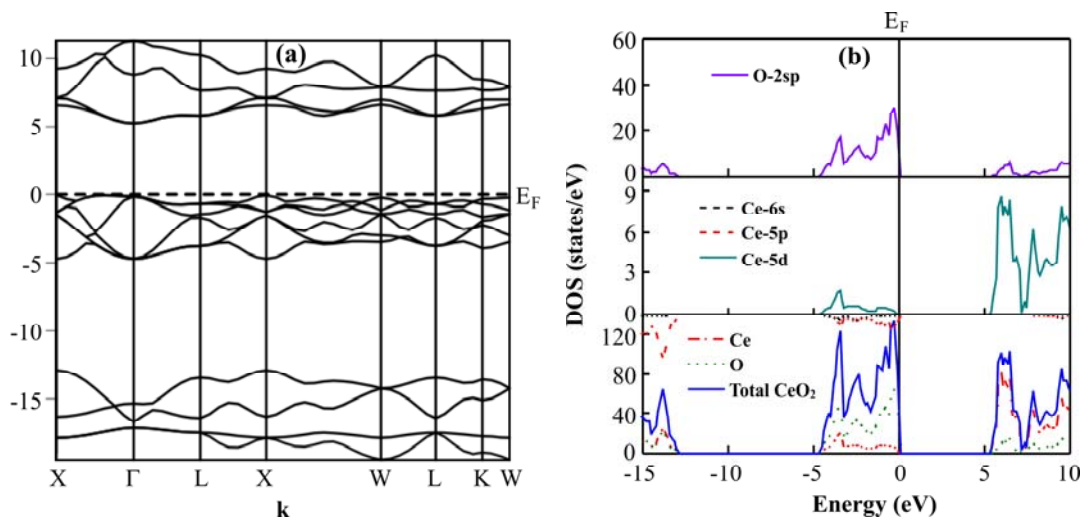


Fig. 2: (a) Energy bands of cubic CeO₂ along the high symmetry directions (b) total and partial density of states using PP-DFT- SOGGA scheme

Energy bands of CeO₂ can be divided into two parts. The energy bands below the Fermi energy (E_F) are denser than those present above the E_F . The energy bands below the E_F are mainly due to the 2sp states of O atom. A small contribution of 5d electrons of Ce is also visible near the VBM. While the energy bands above this level are mainly originated by the 5d electronic states of Ce atom with a very small contribution of O atoms. Further, it can be seen that the contribution of O atoms in the conduction region is very small. Therefore, we conclude that the 5d electrons of Ce atom and 2sp electron of O atoms play a major role in deciding the magnitude of band gap.

In Table 1, we have collated the band gap values in CeO₂ computed using various schemes in the present work along with available theory and experiments. We have presented band gap between O-2sp and Ce-5d because we used pseudo potential basis set of Ce atom. It is seen that the present band gap is close to experimental value (6.00 eV)²⁷.

Table 1: The band gap (ΔE_g) for CeO₂ compound using various schemes of LCAO-DFT, as mentioned in the text, along with the data available in literature

Method		ΔE_g (eV)	
		O-2p-Ce5d	O-2p-Ce-4f
(i) Present work			
LCAO	DFT-PP-WCGGA	5.27	-
	DFT-PP-PBEsol	5.25	-
	DFT-PP-LDA	5.25	-
	DFT-PP-SOGGA	5.25	-
(ii) Available Theory			
VASP	LDA+U [16]	5.14	2.45
	LDA+U, GGA+U [12]	5.00	2.30
	HSE [10]	7.00	3.30
	LDA [15]	-	2.11
	B3LYP [18]	8.16	3.70
	HH [18]	10.64	7.50
	HHLYP [18]	10.75	7.18
	PBE0 [18]	8.52	4.30
LCAO	B1-WC [18]	7.48	3.18
	LDA [22]	6.36	1.37
	PBE [22]	6.46	1.26
	B3LYP [22]	8.06	2.39
	PBE0 [22]	8.45	2.95
	LDA [26]	5.61	2.00
	PBE [26]	5.64	2.00
	PBE0 [26]	7.93	4.50
	HSE [26]	6.96	3.50
	(iii) Available Experiment	Optical reflectivity [27]	5.5-6.5
XPS, BIS, EELS [28]		-	2.6-3.4

Isotropic and anisotropic compton profiles

In the momentum space representation, EMD (ρ) can be written as the sum of the

squared moduli of the occupied crystalline orbitals in a momentum representation. Mathematically,

$$\rho(\mathbf{p}) = \frac{1}{V_{BZ}} \sum_j \int_{BZ} d\mathbf{k} |\psi_j(\mathbf{k}, \mathbf{p})|^2 \theta[\varepsilon_F - \varepsilon_j(\mathbf{k})], \quad \dots(7)$$

where θ is the step function, ε_F the Fermi energy, the \mathbf{k} -dependent eigen value of the j^{th} orbital and V_{BZ} is the volume of the BZ.

Compton profile is derived by 2-D integration of the $\rho(\mathbf{p})$ over a plane through \mathbf{p} and perpendicular to \mathbf{p} direction. After indicating with p_{\perp} , the general vector perpendicular to \mathbf{p} , we write

$$J(\mathbf{p}) = \int dp'_{\perp} \rho(\mathbf{p} + \mathbf{p}'_{\perp}) \quad \dots(8)$$

In Fig. 3, we have presented the EMDs along [100], [110] and [111] directions using PP-DFT-LDA approach. From the figure, it is seen that EMD along [100] direction is higher at $p_z = 0$ a.u., so we can conclude higher momentum density of electrons in [100] direction than [110] and [111] directions. It is also seen that EMD in [110] and [111] directions are almost same. Therefore, it is seen that among principal directions, [100] direction has more anisotropic character.

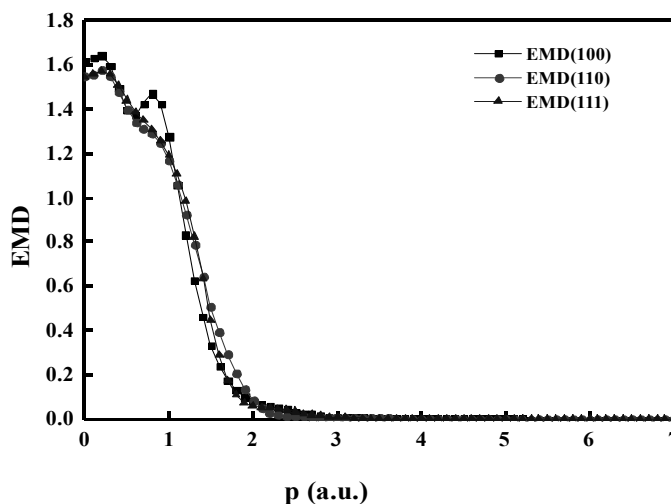


Fig. 3: EMD of CeO₂ along [100], [110] and [111] directions using PP-DFT-LDA scheme

The isotropic valence CP using PP-DFT-WCGGA, PP-DFT-PBEsol, PP-DFT-LDA and PP-DFT-SOGGA for CeO₂ are shown in Fig. 4. It is seen that near $p_z = 0$, the valence CPs of PP-DFT-PBEsol is higher than other theories, which shows less localization of electron in real space when these are dealt with exchange correlation potentials of PBEsol.

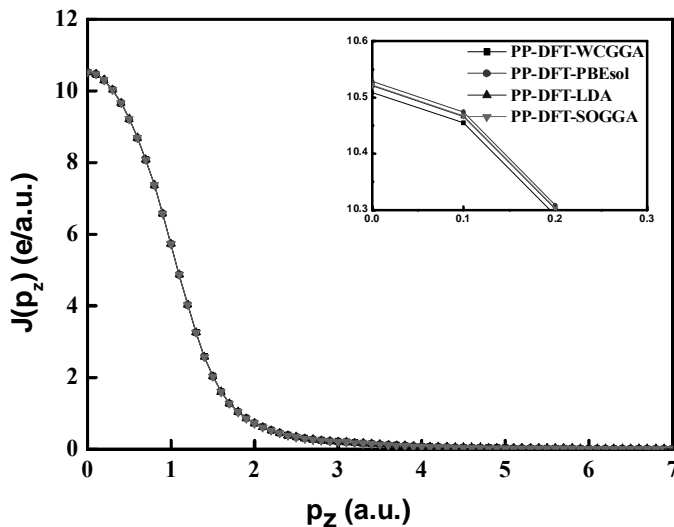


Fig. 4: Isotropic valence compton profile of CeO₂ using PP-DFT-GGA/PBEsol/LDA/SOGGA scheme

The directional differences in momentum densities using PP-DFT-WCGGA, PP-DFT-PBEsol, PP-DFT-LDA and PP-DFT-SOGGA for CeO₂ are shown in Fig. 5. The anisotropies in the directional CPs depict characteristic oscillations, which are governed by the energy bands. A general trend of oscillations in the directional differences $J_{111}-J_{100}$, $J_{111}-J_{110}$ and $J_{110}-J_{100}$ is almost similar, except some fine structures in low momentum region. The anisotropies above the $p_z = 3$ a.u. are hardly visible because this region is dominated by tightly bound core electrons whose momentum densities are cancelled while taking the directional differences. It is also seen that the anisotropies in momentum densities derived from different approximations are almost same. The higher positive value of anisotropy $J_{111}-J_{110}$ near $p_z = 0$ a.u. depicts the higher value of momentum densities along [111] direction than that along [110] direction. We can explain the trend of oscillations in anisotropies in terms of degenerate states along the E_F . For example, anisotropies in $J_{111}-J_{110}$ direction can be explained on the basis of degenerate states in $\Gamma-L$ [111] and $\Gamma-X$ [110] branches. In $\Gamma-L$ branch more degenerate states at Γ point are responsible for higher momentum densities. This leads to positive amplitude of $J_{111}-J_{110}$ in the low momentum region. In the similar way, we can also explain the other positive and negative anisotropies in different directions.

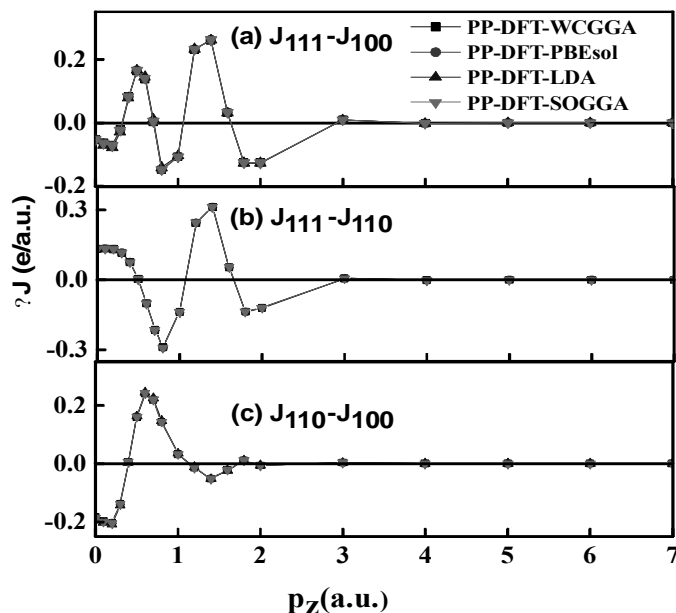


Fig. 5: Anisotropy in the theoretical Compton profiles of CeO₂ calculated using different density functional schemes within the effective pseudo-core potential. Since the statistical error $\pm \sigma$ is within the size of symbols used, it is not clearly visible. The solid lines are drawn to guide the eyes

Measurements on CP of CeO₂ will be helpful to validate the applicability of the exchange and correlation potentials as used in the present investigations.

ACKNOWLEDGMENT

We are thankful to Prof. R. Dovesi for providing the CRYSTAL09 band structure package.

REFERENCES

1. T. Nakazawa, T. Inoue, M. Satoh and Y. Yamamoto, Jpn. J. Appl. Phys., Part I, **34**, 548 (1995).
2. S. Gennard, F. Corá, C. Richard and A. Catlow, J. Phys. Chem. B, **103**, 10158 (1999).
3. N. V. Skorodumova, R. Ahuja, S. I. Simak, I. A. Abrikosov, B. Johansson and B. I. Lundqvist, Phys. Rev. B, **64**, 115108 (2001).
4. N. V. Skorodumova, M. Baudin and K. Hermansson, Phys. Rev. B, **69**, 075401 (2004).

5. Z. Yang, T. K. Woo, M. Baudin and K. Hermansson, *J. Chem. Phys.*, **120**, 7714 (2004).
6. S. Febris, S. de Gironcoli, S. Baroni, G. Vicario and G. Balducci, *Phys. Rev. B*, **71**, 041102 (2005).
7. L. Gerward, J. S. Olsen, L. Petit, G. Vaitheeswaran, V. Kanchana and A. Svane, *J. Alloys Comp.*, **400**, 56 (2005).
8. E. Voloshina and B. Paulus, *J. Chem. Phys.*, **124**, 234711 (2006).
9. V. Kanchana, G. Vaitheeswaran, A. Svane and A. Delin, *J. Phys. Condens. Matt.*, **18**, 9615 (2006).
10. P. J. Hay, R. L. Martin, J. Uddin and G. E. Scuseria, *J. Chem. Phys.*, **125**, 034712 (2006).
11. S. Mehrotra, P. Sharma, M. Rajagopalan and A. K. Bandyopadhyay, *Solid. State. Commun.*, **140**, 313 (2006).
12. C. Loschen, J. Carrasco, K. M. Neyman and F. Illas, *Phys. Rev. B*, **75**, 035115 (2007).
13. P. S. Devi and D. Banerjee, *Ionics*, **14**, 73 (2008).
14. C. Sevik and T. Cagin, *Phys. Rev. B*, **80**, 014108 (2009).
15. M. Fronzi, A. Soon, B. Delley, E. Traversa and C. Stampfl, *J. Chem. Phys.*, **131**, 104701 (2009).
16. J. Kullgren, C. W. M. Castleton, C. Müller, D. M. Ramo and K. Hermansson, *J. Chem. Phys.*, **132**, 054110 (2010).
17. K. K. Babitha, A. Sreedevi, K. P. Priyanka, B. Sabu and T. Varghese, *Ind. J. Pure Appl. Phys.*, **53**, 596 (2015).
18. J. Graciani, A. M. Márquez, J. J. Plata, Y. Ortega, N. C. Hernandez, A. Meyer, C. M. Zicovich-Wilson and J. F. Sanz, *J. Chem. Theory Comput.*, **7**, 56 (2011).
19. P. R. L. Keating, D. O. Scanlon, B. J. Morgan, N. M. Galea and G. W. Watson, *J. Phys. Chem. C*, **116**, 2443 (2012).
20. H. Y. Xiao, Y. Zhang and W. J. Weber, *Phys. Rev. B*, **86**, 054109 (2012).
21. M. B. Kanoun, A. H. Reshak, N. K.-Bouayed and S. G.-Said, *J. Mag. Mag. Mat.*, **324**, 1397 (2012).
22. T. Désaunay, A. Rinduedé, M. Cassir, F. Labat and C. Adamo, *Surface Sci.*, **606**, 305 (2012).

23. H. X. Song, L. Liu, H. Y. Geng and Q. Wu, *Phys. Rev. B*, **87**, 184103 (2013).
24. M. Li, H. Jia, X. Li and X. Liu, *Solid. State. Commun.*, **226**, 8 (2015).
25. R. Gillen, S. J. Clark and J. Robertson, *Phys. Rev. B*, **87**, 125116 (2013).
26. J. L. F. Da Silva, M. V. G.-Pirovano, J. Sauer, V. Bayer and G. Kresse, *Phys. Rev. B*, **75**, 045121 (2007)
27. F. Marabelli and P. Wachter, *Phys. Rev. B*, **36**, 1238 (1987).
28. E. Wuilloud, B. Delley, W.-D. Schneider and Y. Baer, *Phys. Rev. Lett.*, **53**, 202 (1984).
29. D. Mullins, S. Overbury and D. Huntley, *Surface Sci.*, **409**, 307 (1998).
30. R. Dovesi, V. R. Saunders, C. Roetti, R. Orlando, C. M. Zicovich-Wilson, F. Pascale, B. Civalleri, K. Doll, N. M. Harrison, I. J. Bush, Ph D'Arco and M. Llunell, *CRYSTAL09 User's Manual*, University of Torino, Torino (2009).
31. R. Dovesi, R. Orlando, B. Civalleri, C. Roetti, V. R. Saunders and C. M. Zicovich-Wilson *CRYSTAL: Z. Kristallogr.*, **220**, 571 (2005).
32. B. Hammer, L. B. Hansen and J. K. Norskov, *Phys. Rev. B*, **59**, 7413 (1999).
33. Y. Zhao and D. G. Truhlar, *J. Chem. Phys.*, **128**, 184109 (2008).
34. M. D. Towler, A. Zupan and M. Causa, *Comp. Phys. Commun.*, **98**, 181 (1996).
35. Z. Wu and R. E. Cohen, *Phys. Rev. B*, **73**, 235116 (2006).
36. J. P. Perdew, A. Ruzsinszky, G. I. Csonka, O. A. Vydrov, G. E. Scuseria, L. A. Constantin, X. Zhou, K. Burke, *Phys. Rev. Lett.*, **100**, 136406 (2008).
37. J. P. Perdew, K. Burke and M. Ernzerhof, *Phys. Rev. Lett.*, **77**, 3865 (1996).
38. D. D. Johnson, *Phys. Rev. B*, **38**, 12807 (1998).

*Revised : 03.07.2016**Accepted : 04.07.2016*